2008

Hydrogen Peroxide Formation Rates in a PEMFC Anode and Cathode: Effect of Humidity and Temperature

Vijay A. Sethuraman
University of South Carolina - Columbia

John W. Weidner
University of South Carolina - Columbia, weidner@engr.sc.edu

Andrew T. Haug

Sathya Motupally

Lesia V. Protsailo

Publication Info

Journal of the Electrochemical Society, 2008, pages B50-B57.

Publisher's link: http://dx.doi.org/10.1149/1.2801980
DOI: 10.1149/1.2801980

Journal of The Electrochemical Society, **155** (1) B50-B57 (2008)
0013-4651/2007/155(1)/B50/8/$23.00 © The Electrochemical Society

Hydrogen Peroxide Formation Rates in a PEMFC Anode and Cathode

Effect of Humidity and Temperature

Vijay A. Sethuraman,[a,c,*] John W. Weidner,[a,,z] Andrew T. Haug,[b,d,**] Sathya Motupally,[b] and Lesia V. Protsailo[b,**]**

[a]*Center for Electrochemical Engineering, Department of Chemical Engineering, University of South Carolina, Columbia, South Carolina 29208, USA*
[b]*UTC Power, South Windsor, Connecticut 06074, USA*

Hydrogen peroxide (H_2O_2) formation rates in a proton exchange membrane fuel cell (PEMFC) anode and cathode were estimated as a function of humidity and temperature by studying the oxygen reduction reaction (ORR) on a rotating ring disk electrode. Fuel cell conditions were replicated by depositing a film of Pt/Vulcan XC-72 catalyst onto the disk and by varying the temperature, dissolved O_2 concentration, and the acidity levels in hydrochloric acid ($HClO_4$). The $HClO_4$ acidity was correlated to ionomer water activity and hence fuel cell humidity. The H_2O_2 formation rates showed a linear dependence on oxygen concentration and square dependence on water activity. The H_2O_2 selectivity in ORR was independent of oxygen concentration but increased with the decrease in water activity (i.e., decreased humidity). Potential dependent activation energy for the H_2O_2 formation reaction was estimated from data obtained at different temperatures.
 [DOI: 10.1149/1.2801980]

Manuscript submitted July 9, 2007; revised manuscript received September 26, 2007. Available electronically November 8, 2007.

Proton exchange membrane fuel cell (PEMFC) technology, owing to its high efficiency, operational flexibility, and superior modularity, has the capability to be the structural and fundamental unit of an impending hydrogen economy. Two main issues that impede its progress toward commercialization are cost and durability. The U.S. Department of Energy's (DOE) projected performance requirements[1] for the year 2010 are 5000 h (with 20,000 start/stops) at \$45/kW for automotive stacks and upwards of 40,000 h at \$400–\$750/kW for stationary power plants. In addition, current engineering requirements demand stack operation at higher temperatures (>100°C) and low relative humidities (<75% RH). Elevated temperature operation offers better tolerance to CO, faster oxygen reduction reaction (ORR) kinetics, and better water and thermal management enabling easier system integration. However, elevated temperatures and the desire to operate at ambient pressures means the fuel cell needs to be operated at lower relative humidities. Since much of ionomer and membrane technologies have evolved around the water dependent perfluorinated systems such as Nafion, both high temperature and low humidity conditions cause severe performance degradation[2-8] and remain an impediment toward achieving DOE's performance and durability targets.

One of the mechanisms for catalyst/ionomer chemical degradation in PEMFCs involves the formation of hydroxyl and hydroperoxyl (OH· and OOH·) radicals[9,10] caused by hydrogen peroxide (H_2O_2) formation on the catalyst surface via Reaction 1

$$O_2 + 2H^+ + 2e^- \leftrightarrow H_2O_2 \quad E^0 = 0.695 \text{ V vs SHE} \qquad [1]$$

and subsequent decomposition via Reactions 2 and 3. Using a novel in situ spin trap electron paramagnetic resonance study,[11] Panchenko et al.[12] reported no evidence of OH· and OOH· radicals in the anode. They observed the presence of radicals in the cathode and near the membrane-cathode interface. Therefore, the H_2O_2 diffuses into the membrane and chemically breaks down to hydroxyl radicals and ions on metal ions present[13] in the membrane

$$H_2O_2 + M^{2+} \rightarrow M^{3+} + OH\cdot + OH^- \qquad [2]$$

$$OH\cdot + H_2O_2 \rightarrow OOH\cdot + H_2O \qquad [3]$$

These radicals react with the perfluorosulfonic acid type ionomer in the electrode and the membrane to produce hydrofluoric acid (HF).[14] The sequence is listed below

$$R_p - CF_2COOH + OH\cdot \rightarrow R_p - CF_2 + CO_2 + H_2O \qquad [4]$$

$$2R_p - CF_2 + 2OH\cdot \rightarrow R_p - CF_2OH + R_p - COF + HF \qquad [5]$$

$$R_p - COF + H_2O \rightarrow R_p - COOH + HF \qquad [6]$$

The fluoride emission rate is a measure of membrane degradation given in Eq. 5 and 6. Since two-thirds of Nafion is fluorine (on a mass basis), this chemical degradation results in mechanical instability in the membranes causing pinholes and eventual failure. Since this degradation is initiated by the peroxide-radical attack, understanding H_2O_2 kinetics at the electrocatalyst/ionomer interface at low humidities and elevated temperatures from a PEM fuel cell context is vital toward explaining the increased degradation rate observed under such conditions. Though Liu and Zuckerbrod[15] have reported a method for in situ detection of H_2O_2 formation, it only served as a qualitative indicator of the existence of peroxide. In situ quantification of peroxide kinetics is very difficult owing to its instability.

Rotating ring disk electrode (RRDE) studies on supported Pt catalysts have been successfully used[16-21] as a technique to quantify peroxide formation and for screening oxygen reduction catalysts. Paulus et al.[16,18] reported the use of a thin-film RRDE method for characterizing oxygen reduction reaction (ORR) in supported high surface area catalysts and were able to quantify the amount of H_2O_2 produced during the ORR. They decreased the film thickness and improved the ionomer-catalyst film stability at higher rotation speeds, which resulted in uniform collection efficiencies and better peroxide measurements. Antoine and Durand[19] reported a weak platinum particle size effect on H_2O_2 production during ORR and agreed with previously reported observations that H_2O_2 yields were higher for potentials less than 0.4 V vs the standard hydrogen electrode (SHE). Enayetullah et al.[20] studied ORR electrocatalysis on polycrystalline Pt microelectrodes in various concentrations of trifluoromethane sulfonic acid (TFMSA). They reported higher Tafel slopes and lower activation energies for ORR in higher concentrations of TFMSA, which was attributed to lower water activity. Murthi et al.[21] studied ORR in supported Pt and Pt alloy catalysts in 1 M and 6 M TFMSA as a way to study the effect of water activity. They reported higher peroxide yields in 6 M TFMSA solution compared to a 1 M solution. However, none of these studies correlate

* Electrochemical Society Student Member.
** Electrochemical Society Active Member.
[c] Present address: Environmental Energy Technology Division, Lawrence Berkeley National Laboratory, Berkeley, CA 94720, USA.
[d] Present address: 3M Fuel Cell Components, 3M Center, St. Paul, MN 55144.
[z] E-mail: weidner@engr.sc.edu

the measured peroxide yields and selectivity to peroxide formation rates in a PEM fuel cell as a function of cell operating conditions.

Therefore, the objective of this investigation was to predict H_2O_2 formation rates in a PEM fuel cell. This was accomplished by measuring H_2O_2 formation rates at rotating ring disk electrode (RRDE). Fuel cell conditions were replicated by depositing a film of Pt/Vulcan XC-72 catalyst onto the disk and by varying the temperature, dissolved O_2 concentration, and the acidity levels in $HClO_4$. The $HClO_4$ acidity was correlated to ionomer water activity and hence fuel cell humidity. Peroxide formation rate in the anode was predicted using oxygen permeability measured across Nafion 112 membrane and the fraction of oxygen that reduces the H_2O_2. Peroxide formation rate in the cathode was predicted using the rate constants measured from RRDE experiments and the local concentrations of oxygen and protons.

Experimental

Rotating ring disk electrode (RRDE).— For the RRDE studies, commercially available Pt/Vulcan catalyst (20% Pt on Vulcan XC-72R carbon, Johnson Matthey Inc., West Chester, PA) was used. Catalyst coated glassy carbon electrodes were prepared as described by Schmidt et al.[22] Aqueous suspensions of 1 mg catalyst mL^{-1} were obtained by pulse-sonicating 20 mg Pt/Vulcan catalyst with 20 mL triple-distilled, ultrapure water (Millipore Corp.) in an ice bath (70% duty cycle, 60 W, 15 min). Sonication was done using a Braun-Sonic U type 853973/1 sonicator. A glassy carbon disk served as the substrate for the supported catalyst and was polished to a mirror finish (0.05 μm deagglomerated alumina, Buehler) prior to catalyst coating. An aliquot of 14 μL catalyst suspension was pipetted onto the carbon substrate, which corresponded to a Pt loading of $\sim$14.1 μg Pt cm^{-2}. After evaporation of water for 30 min in N_2 atmosphere (381 mm Hg, vacuum), 14 μL of diluted Nafion solution (5% aqueous solution, 1100 EW; Solution Technology Inc., Mendenhall, PA) was pipetted on the electrode surface and further evaporated for 30 min in N_2 atmosphere (381 mm Hg, vacuum). Nafion was used to adhere the Pt/Vulcan particles onto the glassy carbon electrode (the ratio of H_2O/Nafion solution used was $\sim$100/1). Previous work by Paulus et al. indicates that this procedure yielded a Nafion film thickness of $\sim$0.1 μm and that the utilization of the Pt/Vulcan catalyst (based on H-adsorption charge) on the electrode with this film was $\sim$100%.

The catalyst-Nafion coated electrode was immersed in deaerated [ultrahigh purity (UHP) nitrogen, Praxair] perchloric acid ($HClO_4$, 70% ULTREX II ultrapure reagent grade, J. T. Baker) of varying concentrations for further synchronized chronoamperometric and potentiodynamic experiments. Though a variety of supporting electrolytes are reported in the literature, anion adsorption on Pt is minimal for only a few electrolytes.[23] [e.g., trifluoromethane sulfonic acid (TFMSA) and $HClO_4$]. In addition, the ultrapure reagent grade $HClO_4$ used in this study is free of ionic impurities; especially since Cl^- ions, even in trace amounts (i.e., 1 ppm), are shown to drastically change both the activity and the reaction pathway of ORR on Pt catalysts.[23-25] All RRDE experiments were performed at atmospheric pressure and all solutions were prepared from ultrapure water (Millipore Inc., 18.2 MΩ cm).

The electrochemical measurements were conducted in a standard electrochemical cell (RDE Cell, Pine Instrument Company, Rayleigh, NC) immersed in a custom-made jacketed vessel, the temperature of which was controlled by a refrigerated/heating circulator (Julabo Labortechnik GMBH). A ring-disk electrode setup with a bi-potentiostat (Bi-Stat, Princeton Applied Research Inc., Oak Ridge, TN) was used in conjunction with rotation-control equipment (Pine Instrument Company, Rayleigh, NC). EC-Lab software (version 8.60, Bio-logic Science Instruments, Claix, France) was used to control the bi-potentiostat. The Pt ring electrode was held at 1.2 V vs SHE where the oxidation of peroxide is diffusion limited. The catalyst coated glassy carbon disk electrode (5 mm diameter, 0.1966 cm^2 area, DT21 Series, Pine Instrument Company, Rayleigh, NC) was scanned between 0 and 1.2 V vs SHE to characterize H_2O_2 formation within the potential range relevant to fuel cell operating conditions. Potentials were determined using a mercury-mercurous sulfate (Hg/Hg_2SO_4) reference electrode. All potentials in this study, however, refer to that of the standard hydrogen electrode (SHE). A high-surface area Pt cylindrical mesh (5 mm diameter, 50 mm length) attached to a Pt wire (0.5 mm thick, 5 mm length) was used as the counter electrode.

Effect of oxygen concentration.— The effect of oxygen concentration on ORR and H_2O_2 formation kinetics was studied by varying the concentration of oxygen in the solution. The following three gases were used: oxygen (UHP grade, Praxair), air (Industrial, Praxair) and 10.01% oxygen in nitrogen (Airgas). A gas flow meter (0–500 mL, Dwyer Instruments Inc., Michigan City, IN) was used to control the flow of the gas feed at $\sim$100 mL min^{-1} into the electrolyte. The electrochemical cell was sealed during the experiments to keep air from affecting the concentration of dissolved oxygen in the electrolyte. The concentration of dissolved oxygen in the electrolyte was estimated using the solubility values for oxygen in pure liquid water at 25°C and 101 kPa.[26]

Effect of pH.— The effect of proton concentration on ORR and H_2O_2 formation kinetics was studied by varying the acidity of $HClO_4$ in the 2.0–0.1 M concentration window (~ -0.301–1 pH, assuming $K_a \gg 1$ for $HClO_4$). Between solution changes, the electrochemical cell and its components were washed and boiled in deionized water for 5 h to ensure accurate pH levels. The catalyst-Nafion coated electrode was also cleaned in a sonicator before every experiment with triple distilled ultrapure water.

Collection efficiency.— Standard procedure[27] for the determination of collection efficiency of a ring-disk electrode was followed. The electrodes were prepared as described above. The experiment was carried out in an electrochemical cell in deaerated (UHP nitrogen, Praxair) 0.1 M H_2SO_4 (96.5%, J. T. Baker) with 10 mmol L^{-1} $K_3Fe(CN)_6$ (99.7%, J. T. Baker). The disk electrode was swept at 1 mV s^{-1} [vs SHE] while the Pt ring was held at a constant potential of 1.2 V [vs SHE]. At this ring potential, the oxidation of $[Fe(CN)_6]^{4-}$, produced at the disk electrode, to $[Fe(CN)_6]^{3-}$, proceeds under pure diffusion control. The collection efficiency was determined as $N = I_{ring}/I_{disk} = 0.20$, which was independent of disk potential and consistent with the theoretical collection efficiency provided by the manufacturer of the ring-disk electrode.[28]

The two-electron transfer reaction of O_2 reduction to H_2O_2, captured by the Pt ring, was analyzed in this work (see Table I for parameters used in the analysis). At the ring, the H_2O_2 produced at the disk is oxidized via the reverse of Reaction 1. The fraction of H_2O_2 formation, $\chi_{H_2O_2}$, can be determined from the collection efficiency, ring and disk currents by the expression

$$\chi_{H_2O_2} = \frac{2I_{ring}/N}{I_{disk} + I_{ring}/N} \quad [7]$$

The measured current density j corresponding to H_2O_2 formation on a film covered RDE for the first-order ORR kinetics was previously reported to take the following expression,[29] in terms of kinetic and mass-transport dependent currents

$$\frac{1}{j} = \frac{1}{j_{kin}} + \frac{\delta_f}{nFD^f_{O_2}C^f_{O_2}} + \frac{1}{j_D} \quad [8]$$

where j is

$$j = \frac{I_{ring}}{NA} \quad [9]$$

j_{kin} is the current density in the absence of mass transfer effects and j_D is the diffusion current given by the Levich equation

$$j_D = 0.62nFD^{*2/3}_{O_2}C^*_{O_2}\nu^{-1/6}\omega^{1/2} \quad [10]$$

Table I. Parameters used in the analysis of measured current at the Pt ring[a].

Parameter	Value	Comments
a	1	Measured
A	0.164025 cm^2	Ref. 28
b	2	Measured
$C^*_{O_2}$	1.274 mol cm^{-3}	Ref. 26[a]
$D^*_{O_2}$	2.2×10^{-6} cm^2 s^{-1}	Ref. 48
$E^{0'}$	0.695 V vs SHE	
EW	1100 g mol^{-1}	Ref. 49
F	96,485 C mol equiv.$^{-1}$	Ref. 50
N	0.2	Measured
R	8.314 J mol^{-1} K^{-1}	Ref. 50
T^0	298 K	Measured
α	0.5	Assumed
δ_f	10^{-5} cm	Ref. 16
ρ	1 g cm^{-3}	Ref. 50
υ	0.009 cm^2 s^{-1}	Estimated
ω	2500 s^{-1}	Measured

[a] The mole fraction solubility X_l of oxygen in water is given as $\ln X_l = A_2 + (B_2/T^*) + C_2 \ln T^*$, where $T^* = (T/100)K$. $A_2 = -66.7354$, $B_2 = 87.4755$ and $C_2 = 24.4526$.

The concentration of O_2 in the solution was calculated from the partial pressure of O_2 in the inlet gas and O_2 solubility data for pure liquid water at corresponding temperature and 101 kPa.[26] The difference in O_2 solubility in pure liquid water and in $HClO_4$ (up to 2 M) was assumed to be negligible. Combining Eq. 8 and 10 and solving for j_{kin} gives

$$j_{kin} = \frac{jnFD^f_{O_2}C^f_{O_2}D^{*2/3}_{O_2}C^*_{O_2}\omega^{1/2}}{nFD^f_{O_2}C^f_{O_2}D^{*2/3}_{O_2}C^*_{O_2}\omega^{1/2} - \delta_f jD^{*2/3}_{O_2}C^*_{O_2}\omega^{1/2} - 1.6\nu^{1/6}jD^f_{O_2}C^f_{O_2}} \quad [11]$$

The purely kinetic portion of the H_2O_2 formation rate is

$$R_{H_2O_2} = \frac{j_{kin}}{2F} = k_f(C_{O_2})^a(C_{H^+})^b \quad [12]$$

where

$$k_f = k^0_f \exp\left[\frac{\alpha F\eta}{RT^0}\right] \quad [13]$$

In Eq. 12, a and b are reaction orders with respect to O_2 and H^+, respectively. Only the forward rate term is used in Eq. 12 because at 0.6 V vs SHE and below, the rate of oxidation of H_2O_2 (the reverse reaction) is negligible. The kinetic rate constant k_f was estimated for different potentials by plotting H_2O_2 production rate as a function of oxygen concentration for various potentials. Since the electrode reaction rate was shown earlier by Damjanovic and Hudson[30] to be faster on an oxide-free Pt surface than on an oxide-covered surface, both the forward and the reverse scans were used to estimate the reaction rate constant. The potential dependence of this rate constant is given in Eq. 13.

The activation energies for hydrogen peroxide formation reaction were evaluated by using the Arrhenius equation[31] shown below,

$$k^0_f = k^0_{f,0} \exp\left[\frac{E_a}{RT}\right] \quad [14]$$

The activation energies for H_2O_2 formation on supported Pt catalysts were compared to the computationally estimated activation energies reported in the literature. For example, using density functional theory, Anderson and Albu,[32] Sidik and Anderson,[33] and Wang and Balbuena[34] have reported activation energies for H_2O_2 formation on Pt_1, Pt_2, and Pt_3 sites, respectively.

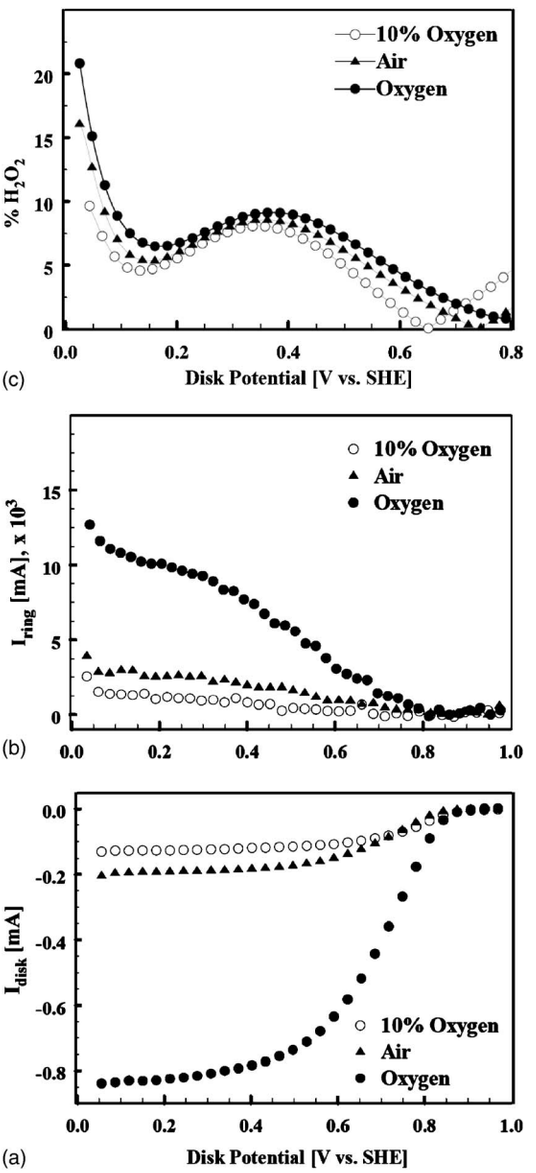

Figure 1. (a) Polarization curves for the oxygen reduction reaction on a Pt/Vulcan XC-72R (14.1 μg Pt cm^{-2}) thin-film RRDE [2500 rpm] in 2.0 M $HClO_4$ solution [pH −0.3] bubbled with 10% O_2 [○], air [▲] and O_2 [●]. (b) Ring currents corresponding to H_2O_2 oxidation [E_{ring} = 1.2 V vs SHE]. (c) % H_2O_2, given by Eq. 11, formed during the oxygen reduction reaction on Pt/Vulcan XC-72R in 2.0 M $HClO_4$ solution [pH −0.3] bubbled with 10% O_2 [○], air [▲] and O_2 [△] at 25°C. E_{ring} = 1.2 V vs SHE, 1 mV/s, 2500 rpm.

Results and Discussion

H_2O_2 kinetic studies using RRDE.— Figure 1a shows polarization curves for the oxygen reduction reaction and Fig. 1b shows ring currents corresponding to H_2O_2 oxidation. It should be noted that hydrogen evolution starts in the neighborhood of ~25–50 mV vs SHE. Hence, both ring and disk currents in the 25–50 mV region include a fractional contribution due to hydrogen evolution [$2H^+ + 2e^- \rightarrow H_2$] and oxidation [$H_2 \rightarrow 2H^+ + 2e^-$] respectively. This is noted by the decrease in the disk currents and an increase in the ring currents in the 25–50 mV potential region. Data obtained below 25 mV were not used in this analysis. Figure 1c shows the fraction

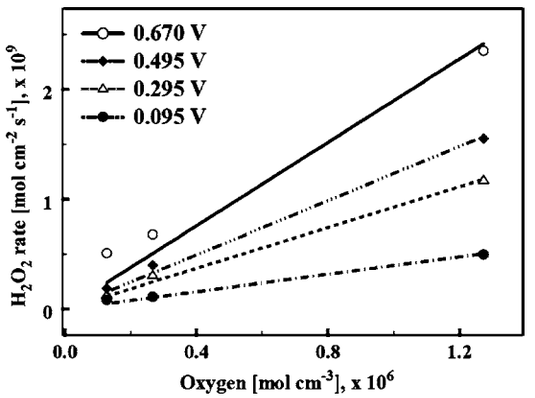

Figure 2. H_2O_2 formation rates [mol cm^{-2} s^{-1}] on Pt/Vulcan XC-72R in 2.0 M $HClO_4$ solution [pH − 0.3] as a function of dissolved oxygen concentration [mol L^{-1}] for the following four overpotentials: 0.695 V [○], 0.495 V [♦] , 0.295 V [△] and 0.095 V [●]. The symbols represent data and the lines represent linear fits with zero intercepts.

of peroxide produced in the ORR at the disk, as captured by the ring and shows no dependence on oxygen concentration.

Figure 2 shows the purely kinetic portion of H_2O_2 formation rates obtained from Eq. 12 as a function of oxygen concentration in the 2 M $HClO_4$ for different overpotentials. The data show a linear dependence of the oxygen concentration at all potentials (i.e., a = 1). In this figure, overpotential of 0.670 V represents a potential of 0.025 V vs SHE because the equilibrium potential for H_2O_2 formation is 0.695 V. Four representative overpotentials were chosen for this plot. The anode experiences the highest overpotential for peroxide formation during fuel cell operation. The cathode potential is above the H_2O_2 equilibrium potential at open circuit but experiences a significant drop during load conditions, and can go negative of H_2O_2 equilibrium potential.

Figure 3 shows the potential dependence of the rate constants estimated from Eq. 12. The 25°C data between η values 0–0.3 V and 0.3–0.65 V was fit with two separate linear equations in Fig. 3. The respective intercepts represent k_f^0 (Eq. 13) and are independent of C_{H^+}. These values, as a function of T, were used to obtain activation energy.

Figure 4 shows the ring currents and the fraction of H_2O_2 formed with different acidities. Perchloric acid systems in the 0.1 and 2.0 M concentration range equilibrated with pure O_2 were used to study the

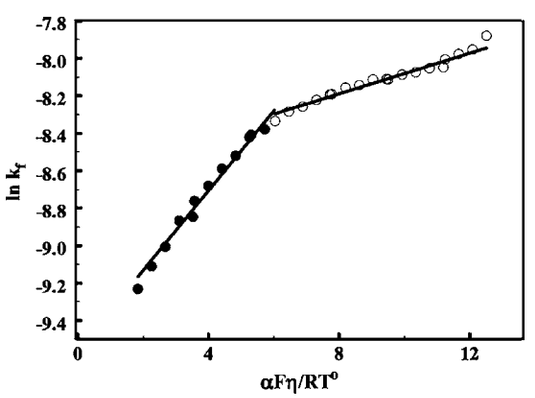

Figure 3. Electrochemical rate constant for H_2O_2 formation, k_f, as a function of overpotential, $\eta = E_{app} - E^0$, E^0 = 0.695 V vs SHE. The data between η values 0–0.3 V and 0.3–0.65 V were fit with two separate linear equations. The value of α = 0.05, T = 25°C. Data was obtained in 2 M $HClO_4$ bubbled with pure O_2 at 1 atm.

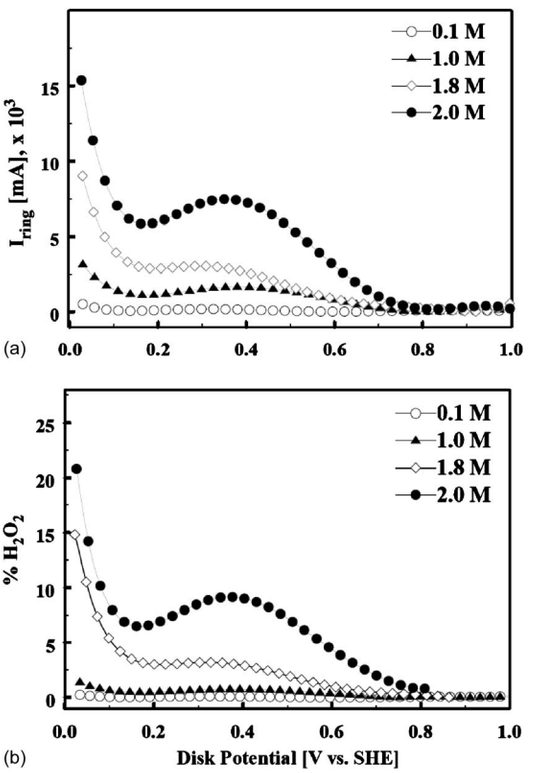

Figure 4. (a) Rate and (b) % of H_2O_2 formed during the oxygen reduction reaction on Pt/Vulcan XC-72R in 0.1 M [○], 1.0 M [▲], 1.8 M [◇] and 2.0 M [●] $HClO_4$ solution [pH −0.3] bubbled with O_2 at 25°C. E_{ring} = 1.2 V vs SHE, 1 mV/s, 2500 rpm.

effect of proton concentration. Figure 4 shows an increased rate of H_2O_2 formation with increasing proton concentration. Since the disk currents were similar for all acid concentrations, the increased ring currents meant that selectivity toward peroxide formation was a function of proton concentration.

Figure 5 shows the dependence of H_2O_2 formation rate on proton concentration. This is consistent with the RRDE results of Murthi et al. in 1 and 6 M TFMSA. The points are measurements and lines are predictions according to Eq. 12. The reaction order with respect to H^+ in the H_2O_2 formation reaction was found to best fit the data for

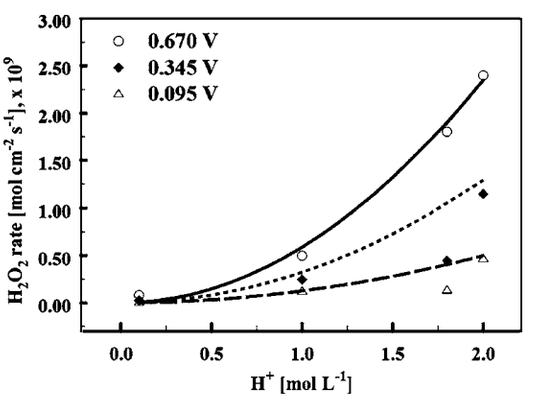

Figure 5. Mass transport corrected H_2O_2 formation rates [mol cm^{-2} s^{-1}] on Pt/Vulcan XC-72R in $HClO_4$ solution as a function of acidity [M] for the following three overpotentials: 0.695 V [○], 0.345 V [♦] and 0.095 V [△]. The lines are predictions according to Eq. 13. The reaction order with respect to H^+ in the H_2O_2 formation reaction, b = 2.

$b = 2$. The reason for the change in selectivity shown by the Pt catalyst in favor of the two-electron transfer at higher acid concentrations (or lower water activities) is beyond the scope of this article. There is a possibility that the adsorption of ClO_4^- anions could influence the reaction pathway in ORR on Pt catalysts similar to that of Cl^- anions as previously reported by Schmidt et al.,[23] Stamenkovic et al.,[25] and Markovic and Ross.[24] However, the bond strength of ClO_4^- adsorption on Pt is much weaker than Cl^- and SO_4^{2-} and its influence on the reaction pathway of ORR is also very minimal.[23,25]

The H_2O_2 formation rates measured as a function of water activity, potential, and temperature using RRDE experiments was used to predict H_2O_2 formation rates at the anode and cathode of PEM fuel cell. Peroxide formation rate at the anode was predicted using oxygen permeability from the cathode and $\chi_{H_2O_2}$. Peroxide formation rate at the cathode was predicted via Eq. 12, i.e., as a product of the rate constant and the local reactant concentrations. Peroxide formation at the cathode occurs only for fuel cells operating under considerable load (i.e., high cell current) such that the local potential goes negative relative to the equilibrium potential for peroxide formation. For estimation of peroxide rates, local potential at the cathode was taken to be 0.6 V (i.e., $\eta = 0.095$ V).

Nafion is a super-acid catalyst and hence the local acidity at the catalyst-membrane interfaces was calculated from the local water content and the fixed number of sulfonic acid groups. The water sorption properties of Nafion as a function of temperature and water activity had been studied by several laboratories.[33-37]

Using a tapered element oscillating microbalance technique, Jalani et al.[37] measured water uptake in Nafion as a function of water activity in vapor phase between 30 and 110°C and reported that the water uptake increased with temperature and was highest at 110°C. The difference in water uptake between 30°C and 110°C is negligible for lower water activities ($a_w < 0.7$). This is reported by Jalani et al. (experimental) and discussed in detail by Motupally et al. (simulations).[40] For this work, the absorption isotherm of Nafion 117 membranes measured at 30°C by Zawodzinski et al.[38,39] was used. Between water activity values of 0 and 1, the experimentally measured absorption isotherm was fit to the following polynomial[41]

$$\lambda = 0.043 + 17.81[a_w] - 39.85[a_w]^2 + 36.0[a_w]^3 \qquad [15]$$

In this equation, λ represents the number of water molecules per sulfonic acid group in the polymer and a_w represents the activity of water, which is the effective mole fraction of water given by p_0/p^*, where p^* is the vapor pressure of water, in bar; p^* was calculated from the Antoine correlation

$$\ln p^* = A_1 - \frac{B_1}{T + C_1} \qquad [16]$$

The constants are $A_1 = 11.6832$, $B_1 = 3816.44$, $C_1 = -46.13$.[42] Inside a fuel cell, this water activity is essentially the equilibrium relative humidity expressed as a fraction. The concentrations of H_2O and H^+ in the polymer are, respectively, expressed as

$$C_{H_2O} = \frac{\rho\lambda}{EW} \qquad [17]$$

$$C_{H^+} = \frac{C_{H_2O}}{\lambda} \qquad [18]$$

In these equations, EW is the equivalent weight of the polymer (taken to be 1100) and ρ is the humidity-dependent density of the polymer given by

$$\rho = \frac{1.98 + 0.0324\lambda}{1 + 0.0648\lambda} \qquad [19]$$

It was assumed that all sulfonic acid groups exist in a completely dissociated form. Figure 6 shows the variation of λ and pH of Nafion as a function of water activity. Even at vapor-saturated conditions [$\lambda = 14$], the pH of Nafion is below 0. This trend (not shown) is seen for $HClO_4$, also a strong acid. The acid was assumed to be completely dissociated i.e., Ka $\gg$ 1. This approach in relating membrane electrode assembly acidity to water activity and hence to the humidity of the incoming gases facilitates in computing peroxide rates inside a fuel cell. Quantitatively, the measured peroxide rates via the RRDE experiments at a particular oxygen concentration, pH value, and temperature should equal the peroxide rates inside the fuel cell at the same pH value and temperature. Since rate constants were measured at 25°C using RRDE, they had to be estimated at higher temperatures in order to be used to calculate peroxide formation rates in a fuel cell. Activation energies for H_2O_2 formation on supported Pt catalysts were estimated from kinetic currents obtained at 15, 25, 35, and 45°C. Figure 7 shows the Arrhenius plot of the logarithmic pre-exponential term k_f^0 vs the inverse of temperature for the two overpotential regions (0–0.3 V and 0.3–0.65 V). The activation energies were obtained from the slope (E_a/R) of a linear fit according to Eq. 14. This procedure is analogous to those described by Neyerlin et al.[43] and Bard and Faulkner.[44]

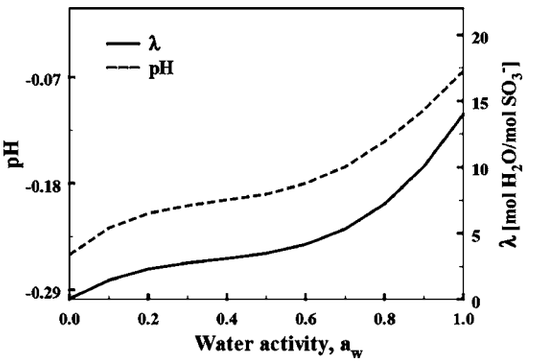

Figure 6. (a) pH (-----) and λ (—) vs water activity, a_w, plots for Nafion; λ is the amount of water per sulfonic acid group [mol basis] and a_w is the effective mole fraction of water and is equal to the equilibrium relative humidity expressed as a fraction.

Oxygen flux across Nafion at higher temperatures.— Oxygen permeability through Nafion depends greatly on the water content of the membrane. It has been shown by Sakai et al.[45] that O_2 diffusion rates in a completely dry Nafion membrane have values similar to that in polytetrafluorethylene and approaches the limit of liquid water with increasing water content. Figure 8 shows experimentally measured O_2 permeability, corrected for an O_2 feed at 101 kPa, across a Nafion 112 membrane as a function of temperature and relative humidity. These permeation rates were estimated using electrochemical monitoring technique and are comparable to those esti-

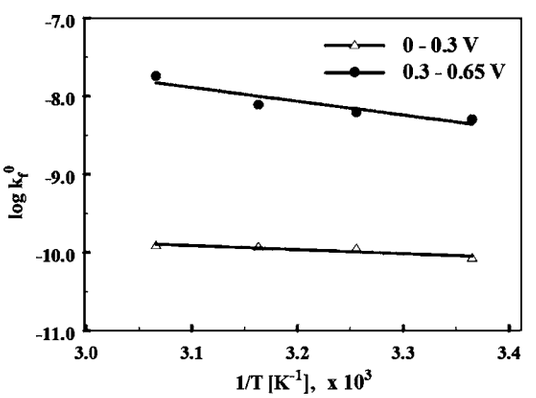

Figure 7. Arrhenius plots for H_2O_2 formation reaction on Pt/Vulcan XC-72R in 2 M $HClO_4$ at overpotential of 0.195 V (-△-) and 0.695 V (-●-) vs NHE.

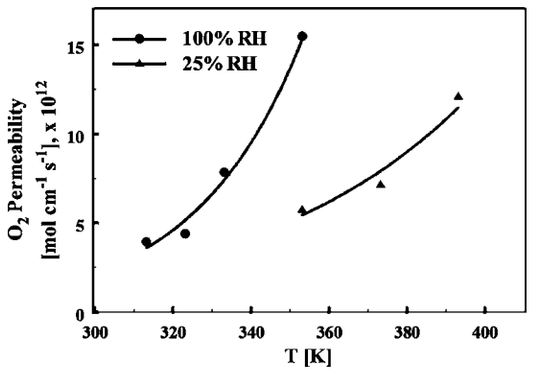

Figure 8. Oxygen permeability [mol cm^{-1} s^{-1}] in Nafion 112 measured by electrochemical monitoring technique as a function of temperature for two different relative humidities, 25% and 100% RH. These rates were normalized to a 101 kPa O_2 feed.

mated by the gas chromatography method.[46] Between 25% and 100% relative humidity of the feed gas, the permeabilities differ by as much as an order of magnitude. Permeability for other temperatures and water contents were estimated by the following equation which was derived by fitting the measured permeability values

$$P^{m}_{O_2} = (1.002 \times 10^{-14} - 9.985 \times 10^{-15} a_w)\exp[(0.0127 + 2.3467 \times 10^{-2} a_w)T] \quad [20]$$

Oxygen solubility at the membrane-cathode catalyst layer interface, $C^{c}_{O_2}$, was estimated using the following relation

$$C^{c}_{O_2} = \frac{P^{m}_{O_2}}{D^{m}_{O_2}} \quad [21]$$

$D^{m}_{O_2}$ values for different temperatures and relative humidities were obtained from the work of Sakai et al.[45] and was fit to the following expression

$$D^{m}_{O_2} = 9.78 \times 10^{-8} + 3.5 \times 10^{-9} T + 10^{-4} a_w \quad [22]$$

Figure 9 shows the peroxide rates at the cathode-membrane interface when the local potential at the cathode is 0.6 V and the gas feed is pure oxygen at 1 atm. Though the amount of peroxide formed at the cathode is only of the order of few micromoles at fully humidified conditions, the relative difference between dry and fully humidified conditions at 95°C is significant.

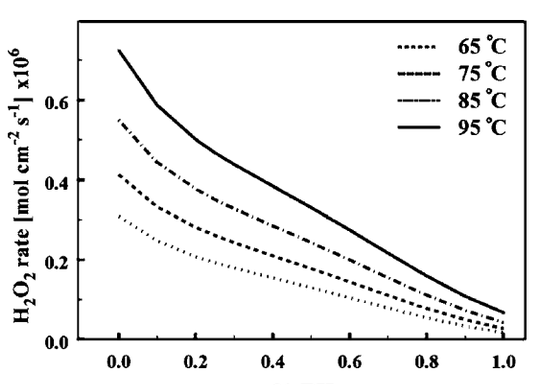

Figure 9. Rates of H_2O_2 formation [mol cm^{-2} s^{-1}] in the cathode side of a PEM fuel cell for different relative humidities and temperatures. Local potential at the cathode was assumed to be ~0.6 V vs SHE, which translates to an overpotential of 0.095 V for H_2O_2 formation.

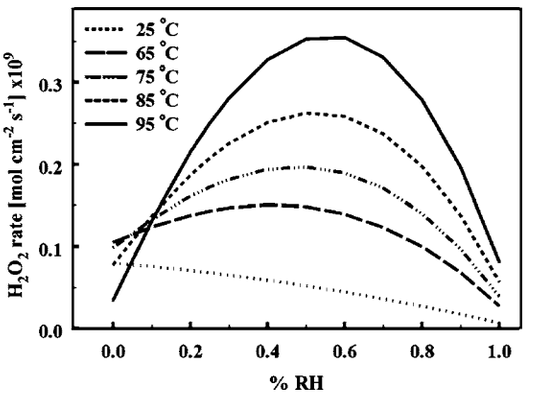

Figure 10. Rates of H_2O_2 formation [mol cm^{-2} s^{-1}] in the anode side of a PEM fuel cell for different relative humidities and temperatures. Local potential at the anode was assumed to be ~0 V vs SHE, which translates to an overpotential of 0.695 V for H_2O_2 formation.

The potential profile across the membrane, measured in situ by Liu and Zuckerbrod[15] (Fig. 19) and modeled by Burlatsky et al.[47] at open circuit conditions, indicates that the potential at the anode-membrane interface is ~0 V. For the purpose of calculating H_2O_2 rates at the anode/membrane interface, a potential of ~0 V (i.e., $\eta = 0.695$ V) was assumed to exist at the interface.

The oxygen flux across the membrane from the cathode to the anode is

$$F_{O_2} = \frac{D^{m}_{O_2}}{\delta}(C^{c}_{O_2} - C^{a}_{O_2}) \quad [23]$$

The concentration of oxygen at the anode-membrane interface approaches zero, assuming all of the oxygen crossing over the membrane to the anode side is reduced to water or reacts chemically with hydrogen

$$R^{a}_{H_2O_2} = \chi_{H_2O_2}\frac{P^{m}_{O_2}}{\delta} \quad [24]$$

While the fraction of oxygen that is reduced to peroxide is a strong function of water activity, it is not a function of oxygen concentration (see Fig. 1c). An expression for $\chi_{H_2O_2}$ vs C_{H^+} was obtained from measured values at room temperature

$$\chi_{H_2O_2} = 0.2081 - 0.1208(a_w) - 0.072(a_w)^2 - 2.132 \times 10^{-14}(a_w)^3 \quad [25]$$

Figure 10 shows the H_2O_2 formation rates at the anode-membrane interface. This goes through a peak because oxygen permeability decreases with decreasing water activity, whereas H_2O_2 selectivity increases with decrease in water activity.

These anode and cathode H_2O_2 formation rates cannot be directly correlated with the fluoride emission rates because there are several intermediate reactions between H_2O_2 formation and actual membrane degradation. Though additional mechanisms involving direct radical formation on Pt followed by their chemical attack on the membrane were suggested,[47] they need further experimental validation and verification. However, quantification of H_2O_2 formation rates described in this work is important in the mechanistic understanding of membrane degradation. This quantification would help in validating a durability mechanism especially at elevated temperatures and low relative humidities.

Conclusion

H_2O_2 formation rates in a PEM fuel cell anode and cathode were estimated by studying the ORR kinetics on a ring disk electrode. Fuel cell conditions were replicated by depositing a film of Pt/

Vulcan XC-72 catalyst onto the disk and by varying the temperature, dissolved O_2 concentration, and the acidity levels in $HClO_4$. The $HClO_4$ acidity was correlated to ionomer water activity and hence fuel cell humidity. H_2O_2 formation rates showed a linear dependence on oxygen concentration and a square law dependence on water activity. The H_2O_2 selectivity in ORR was independent of oxygen concentration but increased with decrease in water activity (i.e., decreased humidity). Potential dependent activation energy for the H_2O_2 formation reaction was estimated from data obtained at different temperatures. Anode peroxide formation rates are proportional to the oxygen flux from the cathode and were estimated to be three orders of magnitude lower than cathode formation rates for a cell operating under load conditions (i.e., $V \leqslant 0.6$ V).

Acknowledgments

The U.S. Department of Energy supported this work under contract no. DOE-DE-FC36-02AL, for which the authors are grateful. The authors thank Michael Fortin for his help with the experimental setup for oxygen crossover measurements.

The University of South Carolina assisted in meeting the publication costs of this article.

List of Symbols

a	reaction order with respect to O_2 in the H_2O_2 formation reaction
a_w	water activity
A	disk area, cm^2
b	reaction order with respect to H^+ in the H_2O_2 formation reaction
C_{H^+}	proton concentration, mol cm^{-3}
C_{H_2O}	water concentration in the membrane, mol cm^{-3}
$C^*_{O_2}$	oxygen concentration in the bulk of the electrolyte, mol cm^{-3}
$C^f_{O_2}$	oxygen concentration in Nafion film, mol cm^{-3}
$C^a_{O_2}$	oxygen concentration in Nafion 112 membrane-anode catalyst layer interface, mol cm^{-3}
$C^c_{O_2}$	oxygen concentration in Nafion 112 membrane-cathode catalyst layer interface, mol cm^{-3}
$D^*_{O_2}$	oxygen diffusion coefficient in the electrolyte, $cm^2\ s^{-1}$
$D^f_{O_2}$	oxygen diffusion coefficient in Nafion film, $cm^2\ s^{-1}$
$D^m_{O_2}$	diffusion coefficient of O_2 in Nafion 112 membrane, $cm^2\ s^{-1}$
E^0	equilibrium potential, 0.695 V vs SHE at 25°C and 101 kPa
E^*_a	activation energy for H_2O_2 formation, J mol^{-1}
E_{app}	applied potential, V vs SHE
EW	equivalent weight of Nafion polymer, 1100 g $equiv^{-1}$
F	Faraday constant, 96,485 C mol^{-1}
I_{ring}	ring current, mA
I_{disk}	disk current, mA
j	total peroxide current density, mA cm^{-2}
j_{disk}	disk current density, mA cm^{-2}
j_D	diffusion-limited current density, mA cm^{-2}
j_{kin}	kinetic current density, mA cm^{-2}
k_b	rate constant for H_2O_2 electro-oxidation, s^{-1}
k_f	rate constant for H_2O_2 formation, $mol^2\ cm^{-5}\ s^{-1}$
N	collection efficiency
n	number of electrons transferred per O_2 molecule in H_2O_2 formation, 2
$P^m_{O_2}$	permeability of O_2 in Nafion 112 membrane, mol $cm^{-1}\ s^{-1}$
R	universal gas constant, 8.314 J $mol^{-1}\ K^{-1}$
T	temperature, K
t	time, s

Greek

α	transfer coefficient
δ	Pt/C electrode thickness, cm
δ_f	Nafion film thickness, cm
ρ	density of Nafion, g cm^{-3}
ν	kinematic viscosity, $cm^2\ s^{-1}$
η	overpotential, V vs SHE
λ	moles of water per sulfonic acid group in Nafion
$\chi_{H_2O_2}$	fraction of O_2 reducing to H_2O_2
ω	electrode rotation rate, s^{-1}

Superscript

0	standard state or equilibrium
a	anode
c	cathode

Subscript

b	backward reaction
D	diffusion
disk	Pt/Nafion coated disk electrode
f	Nafion film or forward reaction
kin	kinetic
ring	Pt ring electrode

References

1. http://www.eere.energy.gov/hydrogenandfuelcells/
2. H. A. Gasteiger, W. Gu, R. Makharia, M. F. Mathias, and B. Sompalli, in *Handbook of Fuel Cells—Fundamentals, Technology and Applications*, Vol. 3, W. Vielstich, A. Lamm, and H. A. Gasteiger, Editors, p. 593, Wiley, New York (2003).
3. D. P. Wilkinson and J. St.-Pierre, *Handbook of Fuel Cells: Fundamentals, Technology and Applications*, Vol. 3, W. Vielstich, A. Lamm and H. A. Gasteiger, Editors, p. 611, Wiley, New York (2003).
4. C. Paik, T. Skiba, V. Mittal, S. Motupally, and T. Jarvi, Abstract 771, The Electrochemical Society Meeting Abstracts, Vol. 2005-1, Quebec City, Canada, May 15–20, 2005.
5. V. Mittal, C. Paik, and S. Motupally, Abstract 772, The Electrochemical Society Meeting Abstracts, Vol. 2005-1, Quebec City, Canada, May 15–20, 2005.
6. S. Hommura, K. Kawahara, and T. Shimohira, Abstract 806, The Electrochemical Society Meeting Abstracts, Vol. 2005-1, Quebec City, Canada, May 15–20, 2005.
7. M. Inaba, H. Yamada, J. Tokunaga, and A. Tasaka, Abstract 1506, The Electrochemical Society Meeting Abstracts, Vol. 2005-1, Quebec City, Canada, May 15–20, 2005.
8. T. Takeshita, F. Miura, and Y. Morimoto, Abstract 1511, The Electrochemical Society Meeting Abstracts, Vol. 2005-1, Quebec City, Canada, May 15–20, 2005.
9. A. B. LaConti, M. Hamdan, and R. C. McDonald, in *Handbook of Fuel Cells—Fundamentals, Technology and Applications*, Vol. 3, W. Vielstich, A. Lamm and H. A. Gasteiger, Editors, p. 647, Wiley, New York (2003).
10. E. Endoh, S. Terazono, H. Widjaja, and Y. Takimoto, *Electrochem. Solid-State Lett.*, **7**, A209 (2004).
11. A. Panchenko, Dipl.-Chem., Institute für Phzsikalische Chemie der Universität Stuttgart (2004).
12. A. Panchenko, H. Dilger, J. Kerres, M. Hein, A. Ullrich, T. Kaz, and E. Roduner, *Phys. Chem. Chem. Phys.*, **6**, 2891 (2004).
13. W. Bi, G. E. Gray, and T. Fuller, *Electrochem. Solid-State Lett.*, **10**, B101 (2007).
14. D. E. Curtin, R. D. Lousenberg, T. J. Henry, P. C. Tangeman, and M. E. Tisack, in *Proceedings of the Second European Polymer Electrolyte Fuel Cell Forum*, Vol. 1, p. 25 (2003); D. E. Curtin, R. D. Lousenberg, T. J. Henry, P. C. Tangeman, and M. E. Tisack, *J. Power Sources*, **131**, 41 (2004).
15. W. Liu and D. Zuckerbrod, *J. Electrochem. Soc.*, **152**, A1165 (2005).
16. U. A. Paulus, T. J. Schmidt, H. A. Gasteiger, and R. J. Behm, *J. Electroanal. Chem.*, **495**, 134 (2001).
17. E. Claude, T. Addou, J.-M. Latour, and P. Aldebert, *J. Appl. Electrochem.*, **28**, 57 (1998).
18. U. A. Paulus, A. A. Wokaun, G. G. Scherer, T. J. Schmidt, V. Stamenkovic, N. M. Markovic, and P. N. Ross, *Electrochim. Acta*, **47**, 3787 (2002).
19. O. Antoine and R. Durand, *J. Appl. Electrochem.*, **30**, 839 (2000).
20. M. A. Enayetullah, T. D. DeVilbiss, and J. O'M. Bockris, *J. Electrochem. Soc.*, **136**, 3369 (1989).
21. V. S. Murthi, R. C. Urian, and S. Mukerjee, *J. Phys. Chem. B*, **108**, 11011 (2004).
22. T. J. Schmidt, H. A. Gasteiger, G. D. Stäb, P. M. Urban, D. M. Kolb, and R. J. Behm, *J. Electrochem. Soc.*, **145**, 2354 (1998).
23. T. J. Schmidt, U. A. Paulus, H. A. Gasteiger, and R. J. Behm, *J. Electroanal. Chem.*, **508**, 41 (2002).
24. N. Markovic and P. N. Ross, *J. Electroanal. Chem.*, **330**, 499 (1992).
25. V. Stamenkovic, N. M. Markovic, and P. N. Ross, Jr., *J. Electroanal. Chem.*, **500**, 44 (2001).
26. L. H. Gevantman, in *CRC Handbook of Chemistry and Physics*, 79th ed., D. R. Lide, Editor, p. 8, CRC, New York (1998–99).
27. W. J. Albery and M. L. Hitchman, *Ring-Disc Electrodes* Clarendon Press, Oxford, United Kingdom, (1971).
28. *Rotated Ring-Disk Electrodes: DT21 Series*, Pine Instrument Company, Raleigh, NC 27617.
29. S. K. Zečević, J. S. Wainright, M. H. Litt, S. Lj. Gojković, and R. F. Savinell, *J. Electrochem. Soc.*, **144**, 2973 (1997).
30. A. Damjanovic and G. Hudson, *J. Electrochem. Soc.*, **135**, 2269 (1988).
31. U. A. Paulus, A. Wokaun, G. G. Scherer, T. J. Schmidt, V. Stamenkovic, V. Radmilovic, N. M. Markovic, and P. N. Ross, *J. Phys. Chem. B*, **106**, 4181 (2002).
32. A. B. Anderson and T. V. Albu, *J. Electrochem. Soc.*, **147**, 4229 (2000).
33. R. A. Sidik and A. B. Anderson, *J. Electroanal. Chem.*, **528**, 69 (2002).
34. Y. Wang and P. B. Balbuena, *J. Chem. Theory Comput.*, **1**, 935 (2005).
35. D. R. Morris and X. Sun, *J. Appl. Polym. Sci.*, **50**, 1445 (1993).
36. D. Rivin, C. E. Kendrick, P. W. Gibson, and N. S. Schneider, *Polymer*, **42**, 623 (2001).
37. N. H. Jalani, P. Choi, and R. Datta, *J. Membr. Sci.*, **254**, 31 (2005).
38. T. Zawodzinski, M. Neeman, L. Sillerud, and S. Gottesfeld, *J. Phys. Chem.*, **95**,

6040 (1991).
39. J. T. Hinatsu, M. Mizuhata, and H. Takenaka, *J. Electrochem. Soc.*, **141**, 1493 (1994).
40. S. Motupally, A. J. Becker, and J. W. Weidner, *J. Electrochem. Soc.*, **147**, 3171 (2000).
41. T. Fuller, Ph.D. Thesis, University of California, Berkeley (1989).
42. R. C. Reid, J. M. Prausnitz, and T. K. Sherwood, *The Properties of Gases and Liquids*, McGraw-Hill, New York (1977).
43. K. C. Neyerlin, W. Gu, J. Jorne, and H. A. Gasteiger, *J. Electrochem. Soc.*, **153**, A1955 (2006).
44. A. J. Bard and L. R. Faulkner, *Electrochemical Methods*, Wiley, New York (1980).
45. T. Sakai, H. Takenaka, and E. Torikai, *J. Electrochem. Soc.*, **133**, 88 (1986).
46. K. Broka and P. Ekdunge, *J. Appl. Electrochem.*, **27**, 117 (1997).
47. S. Burlatsky, T. Jarvi, and V. Atrazhev, Abstract No. 502, The Electrochemical Society Meeting Abstracts, Vol. 2005-2, Los Angeles, CA, Oct 16–21, 2005.
48. Q. Guo, V. A. Sethuraman, and R. E. White, *J. Electrochem. Soc.*, **151**, A983 (2004).
49. K. A. Mauritz and R. B. Moore, *Chem. Rev. (Washington, D.C.)*, **104**, 4535 (2004).
50. R. H. Perry and D. W. Green, *Perry's Chemical Engineer's Handbook*, 7th ed., McGraw-Hill, New York, (1997).